Article

Single Metal Atoms Embedded in the Surface of Pt Nanocatalysts: The Effect of Temperature and Hydrogen Pressure

Qing Wang [1,*,†], Beien Zhu [2], Frederik Tielens [3,*] and Hazar Guesmi [1,*]

1 ICGM, Univ. Montpellier, CNRS, ENSCM, 34095 Montpellier, France
2 Shanghai Institute of Applied Physics, Chinese Academy of Sciences, Shanghai 201800, China
3 Research Group of General Chemistry (ALGC)—Materials Modelling Group, Vrije Universiteit Brussel, Pleinlaan 2, 1050 Brussel, Belgium
* Correspondence: qing.wang@ens-lyon.fr (Q.W.); frederik.tielens@vub.be (F.T.); hazar.guesmi@umontpellier.fr (H.G.)
† Current address: ENSL, CNRS, Laboratoire de Chimie UMR 5182, 46 Allée d'Italie, 69364 Lyon, France.

Abstract: Embedding energetically stable single metal atoms in the surface of Pt nanocatalysts exposed to varied temperature (T) and hydrogen pressure (P) could open up new possibilities in selective and dynamical engineering of alloyed Pt catalysts, particularly interesting for hydrogenation reactions. In this work, an environmental segregation energy model is developed to predict the stability and the surface composition evolution of 24 Metal M-promoted Pt surfaces (with M: Cu, Ag, Au, Ni, Pd, Co, Rh and Ir) under varied T and P. Counterintuitive to expectations, the results show that the more reactive alloy component (i.e., the one forming the strongest chemical bond with the hydrogen) is not the one that segregates to the surface. Moreover, using DFT-based Multi-Scaled Reconstruction (MSR) method and by extrapolation of M-promoted Pt nanoparticles (NPs), the shape dynamics of M-Pt are investigated under the same ranges of T and P. The results show that under low hydrogen pressure and high temperature ranges, Ag and Au—single atoms (and Cu to a less extent) are energetically stable on the surface of truncated octahedral and/or cuboctahedral shaped NPs. This indicated that coinage single-atoms might be used to tune the catalytic properties of Pt surface under hydrogen media. In contrast, bulk stability within wide range of temperature and pressure is predicted for all other M-single atoms, which might act as bulk promoters. This work provides insightful guides and understandings of M-promoted Pt NPs by predicting both the evolution of the shape and the surface compositions under reaction gas condition.

Keywords: single atom Pt nanocatalysts; multi-scaled reconstruction (MSR); stability; DFT; shape & surface composition prediction; reactive condition

1. Introduction

Platinum catalysts are essential in energy, environmental remediation, fine chemicals, data storage, fuel cell, etc. [1,2] However, due to the high price of Pt and its extreme scarcity, the development of alloyed Pt catalysts such as core-shell, Janus or skin-heart structures, [3] allowing for the reduction in the Pt loading amount while preserving or even improving its catalytic efficiency, is of paramount importance. For instance, the very recent work of Liu et al. [4] shows that Au-promoted Pt nanoparticles (NPs) are efficient catalysts for selective oxidation of glycerol. The presence of Au seems to enhance the adsorption and activation of intermediate products. In addition to the selection of the best promoter for a given reaction, the most challenging task remains the control of the surface structure and composition evolutions under reaction conditions which is the most crucial factor governing the catalytic performance of the catalysts. Indeed, it is now well established that the surface of metallic and bimetallic catalysts often undergoes drastic

structural and morphological changes under working conditions [5–10]. Investigated by in-situ and operando experimental technics works [11–13], surface reconstructions and surface or bulk segregation induced by the presence of adsorbates have been shown for a number of bimetallic systems [14–18]. The essential role of adsorbates in the surface restructuring of Cu-based single-atom alloy catalysts was evidenced by K. Yang et al. [5,6]. Ahmadi et al. [14], reported experimental evidence of segregation trends changing in Ni-Pt nanoparticles as a function of reactive gas pressure. Using environmental XPS technics, these authors measured the evolution of Ni/Pt ratio of Ni-Pt NPs exposed to 1 bar of CO. The results show an increase from Ni/Pt ratio of 0.7 at 298 K (Pt-rich) to 1.5 at 673 K (Ni-enriched), followed by a decrease that reaches the value of 0.7 (Pt-rich) at 873 K. In a recent work [18], combining in-situ IR spectroscopy and DFT calculations, we have investigated the evolution of environmental and electronic properties of Sn-promoted Pt nanocatalysts under CO pressure. In contrast with under vacuum conditions where Sn is highly stable on the surface of Sn-Pt, the Pt surface enrichment upon CO exposure was observed by diffuse reflectance Fourier transform infrared (FT-IR) spectroscopy (DRIFTS) and rationalized by the theoretical calculations, which also indicated that isolated Pt was favored over Pt pairing in a Sn-rich alloy. Several theoretical works have investigated the segregation phenomena in alloys in presence of gas [19–22] but stationary approaches have often been considered. After the seminal work of Ruban et al. [23] who established, under vacuum, a database of trends in surface segregation energy (E_{seg}) of single transition metal impurities (solute metal) in transition metals hosts, Greeley et al. [24] performed DFT calculations for segregation energy of hydrogen-related reactions. These authors compared the segregation energy (E_{seg}^{BE}) of the solute metal with the hydrogen binding energy difference between solute and host metal ($\left| BE_H^{sol} \right| - \left| BE_H^{host} \right|$). However, this stationary model does not involve the reaction condition effect (temperature and gas pressure) and by consequence it is not able to describe the dynamic changes of alloy surface composition under working conditions. Very recently, Meng et al. proposed a new model [25] to include the gas coverage and lateral interaction effects on surface segregation (E_{eseg}) evolution for bimetallic alloys under T and P change using DFT combined with the Fowler-Guggenheim isotherm theory. This approach has been shown to be effective for the prediction of the surface composition of several bimetallic alloy systems under varied temperature and pressure.

In addition to surface composition evolution in nanostructured catalysts, shape changes under working conditions have been shown to affect their reactivity [3,7]. Differences in the catalytic performance of Pt nanoparticles toward the oxidation reaction of 2-propanol have been observed for NPs with similar average diameter but different shapes [26] which was explained by geometric effects, with undercoordinated Pt atoms on the NP surface, constituting the most active reaction sites [27–29]. Synergistic effects have also been reported on Pt for the oxygen-reduction reaction, where oxygen adsorption was found to take place on Pt (100) planes, but its reduction occurs at (111) facets after an intermediate step of surface diffusion from the initial adsorption sites [30]. Thus, the identification of the precise shape of Pt-based nanocatalyst at a given temperature and pressure is crucial as the catalytic properties may be dependent on it [25–31].

In this work, we predict the shape changes of Pt-NPs under H_2 reaction condition with varied temperature and pressure. The hydrogen is ubiquitous in many reactions catalyzed by Pt-based catalysts and particularly in hydrogenation and dehydrogenation reactions. Next, we employ the environmental segregation model to evaluate the surface segregation behavior of eight selected metal promoters M (with M = Cu, Ag, Au, Ni, Pd, Co, Rh and Ir). These M promoters are anchored as single atoms in several host Pt surface orientations where hydrogen is adsorbed. The mapped environmental surface segregation (E_{eseg}) trends together with predicted NPs shapes give a picture of the evolution of M-promoted Pt nanocatalysts as a function of hydrogen gas pressure and temperature.

2. Results and Discussions

2.1. Modeling Equilibrium Shape of Pure Pt-NPs under Temperature and Hydrogen Pressure

Table 1 depicts all DFT calculated parameters needed for the MSR construction. As expected, under vacuum, the calculated surface energies of Pt surfaces are found to respect the order of $\gamma_{(111)} < \gamma_{(100)} < \gamma_{(110)}$, which is in full agreement with the literature [32,33]. The most stable calculated hydrogen adsorption energies show that hydrogen strongly adsorbs on the (100) facet and then on the (110) followed by the (111) facets. For the (111) surface, the fcc site is the most favorable adsorption site for atomic hydrogen (−0.70 eV) and on the (100) and the (110) facets it is the bridge site (−0.84 eV and −0.75 eV, respectively). The difference in adsorption energies between the bridge and the fcc sites varies from 0.05 eV to 0.14 eV. This preference of hydrogen to open Pt surfaces is in good agreement with many previously reported studies [34–36]. In order to evaluate the strength of the lateral interaction between hydrogen atom adsorbates, we calculated the evolution of the adsorption energy with increasing coverage on each Pt surface and the results show relatively higher repulsive H-H lateral interaction on Pt (111) (−0.13 eV) than on Pt (100) (−0.063 eV). On Pt (110) the lateral interaction is found to be negligible, which is in agreement with the literature [37].

Table 1. All DFT calculated pre-requisite parameters for MSR construction. Adsorption energies E_{ads}^{hkl}, surface energy γ_{hkl}, lateral interaction zw and atomic area A of Pt calculated by DFT.

Pt	E_{ads}^{hkl} (eV) [a]	zw (eV)	γ_{hkl} (eV/ Å^2)	A (Å^2)
(111)	−0.70	−0.13	0.098	6.85
(100)	−0.84	−0.063	0.12	7.91
(110)	−0.758	0.00	0.13	11.18

[a] The E_{ads}^{hkl}, represents the adsorption energies over the most stable hydrogen adsorption site for each facet.

The pre-requisite parameters ready-in-hand, we modeled, the shape evolutions of Pt-NPs of size around 5 nm containing about 24,000 Pt atoms for temperature changing between 200 and 1200 K, while the hydrogen pressure varies from 1 to 10^5 Pa (1 bar). These temperature and gas pressure ranges may cover most experimental conditions. The individual modeled structures are denoted as Pt-NP_$\overline{CN}_n$.

In Figure 1, the contour plot shows the different Pt-NP structures constructed with MSR model as a function of temperature and hydrogen pressures identified by the different $\overline{CN}$ values and coded with different colors. Thus, the dark red color represents the smallest average coordination number and the purple color indicates the highest average coordination number. In the whole modeling (*T*, *p*)-range, the Pt-NP shape ($\overline{CN}$ values) is found to change between Pt-NP_$\overline{CN}_{7.83}$ (cube-like) and Pt-NP_$\overline{CN}_{8.81}$ (octahedron-like), reflecting the increase/decrease of the fraction of (111)/(100) facet on the Pt-NP surface, respectively. Based on the contour plot, the evolution manner of Pt-NP shapes can be summarized into two modes:

(i) For hydrogen pressure above 10^4 Pa (0.1 bar), marked in white dashed line in Figure 1, the Pt-NP shape evolves progressively from near-perfect octahedron shape (Pt-NP_$\overline{CN}_{8.81}$) to the near-perfect cube (truncated cube) shape (Pt-NP_$\overline{CN}_{7.92}$) when increasing the temperature. In this domain, the fraction of (100) facet increases from 5.5% to 90.7% and the fraction of (111) facet decreases from 94.2% to 9.3%, respectively.

(ii) Bellow hydrogen pressure of 10^4 Pa (0.1 bar), the Pt-NPs are predicted to undergo reversible shape changes with increasing temperature. Indeed, firstly the Pt-NPs changes from near-perfect octahedron to the near-perfect cube shape, then the shapes start to reverse back and stabilize in the form of a truncated octahedral shape, Pt-NP_$\overline{CN}_{8.64}$.
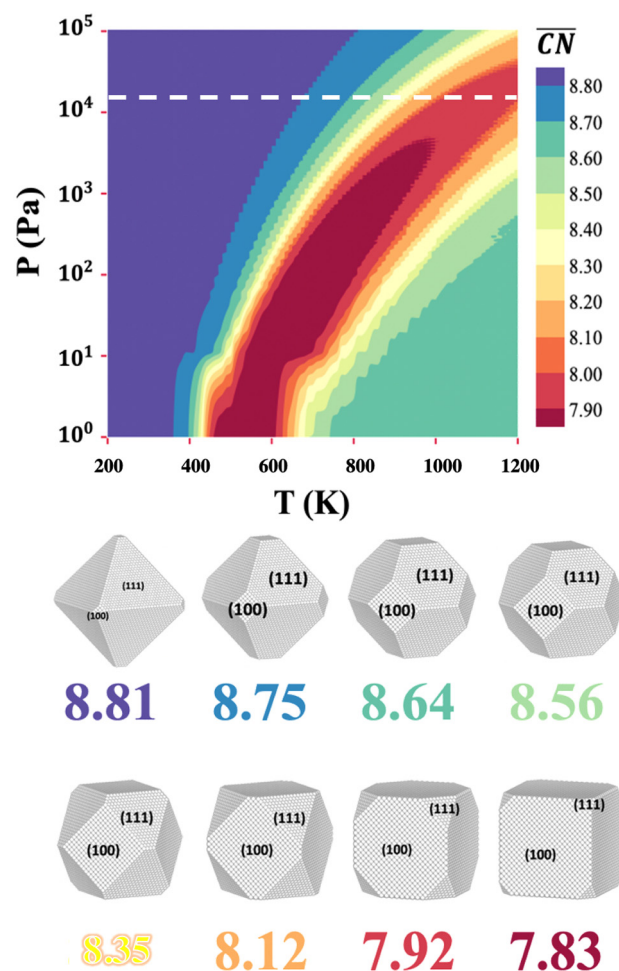
Figure 1. Multiscale Structure Reconstruction (MSR) constructed Pt-NP_$\overline{CN}_n$ under hydrogen environment. The Pt-NP shapes with size of 5 nm as functions of temperatures and hydrogen pressures (upper subfigure), wherein each color represents one different $\overline{CN}$ value which is labeled with different colors. Subfigure on the bottom shows the full sets of color-coded Pt-NP_$\overline{CN}_n$ structures constructed.

In order to understand the above dynamic changes especially the shape reversibility in the lower pressure area, the evolution of hydrogen coverage and the interface tension on each surface facet are computed as a function of temperature. In Figure 2, the results for two different hydrogen pressures, 1 and 0.01 bar are reported (additional results for 0.1 bar pressure are provided in Figure S1). As the morphology changes of NPs are governed by the stability of interface facets and their affinity with the gas environment, the analysis of the evolution of interface energies may provide information on the preferable equilibrium shape. These interface tensions are (T, P, θ)-dependent observables. For Pt NPs exposed to 1 bar (10^5 Pa) of hydrogen pressure (Figure 2A), the hydrogen coverage on (111), (110), and (100) facets are of maximum at low temperature. This indicates that the (111) surface which has the lowest interface tension will remain as the dominant facet of equilibrium Pt-NPs in this temperature region. Next, with the increase of temperature above 1000 K, the H coverage on (111) facet starts to decrease while on the (100) and the (110) facets, the coverage barely decreases. This result is in line with the lower adsorption energy of hydrogen on (111) surface compared to the (100) and (110) ones. Consequently, the interface tension of (111) facet increases faster than that of (100) facet until it becomes higher, which results in the increase of the proportion of the (100) facet at the expense of the (111) facet. Under 0.01 bar (10^3 Pa) of hydrogen pressure (Figure 2B), the fraction of facet (111) is found to rapidly decrease for T above 600 K and reaches the range of 0.3–0.1 mL for T higher

than 1100 K. In that range, the coverage of hydrogen on the three facets is almost equal. Considering the evolution of interface tension, the results show that the (100) facet becomes more stable and thus more dominant than the (111) facet for temperature between 700 and 1100 K. For temperature higher than 1100 K, a shape reversing of Pt-NP is observed.
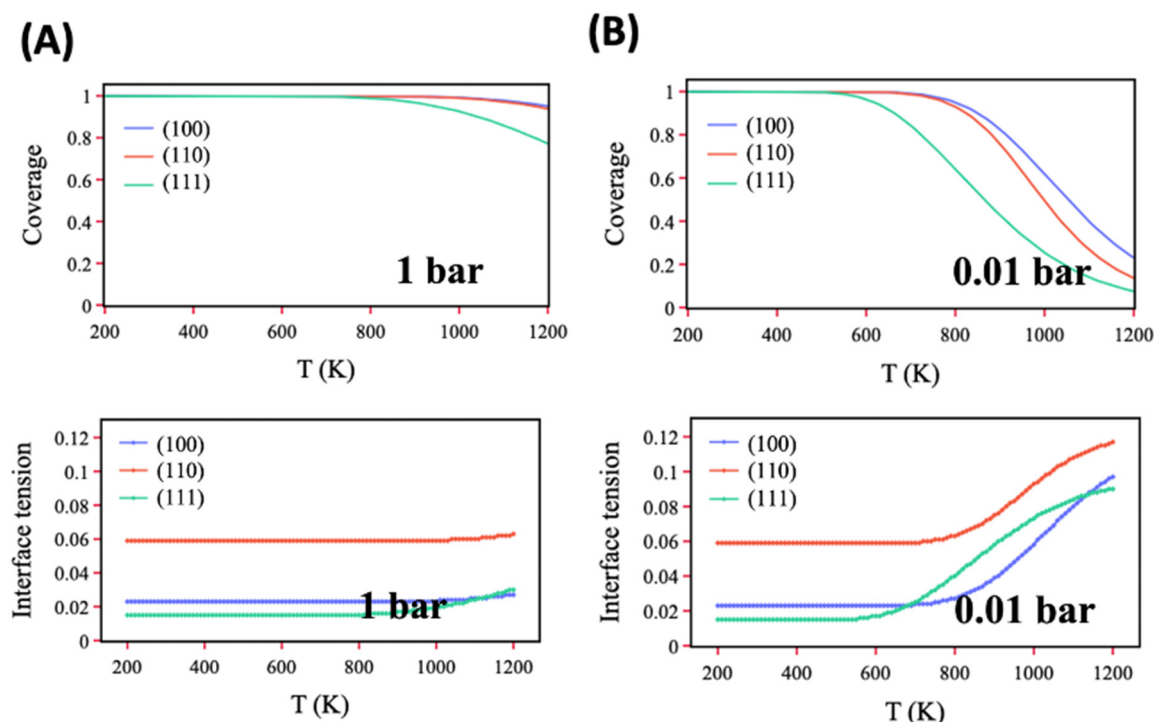
Figure 2. Hydrogen coverage and interface tension (eV/Å^2) evolution profiles of (111), (110) and (100) surface of Pt-NP constructed by MSR model as functions of temperature (**A**) Under 1 bar (10^5 Pa) of hydrogen pressure. (**B**) Under 0.01 (10^3 Pa) bar of hydrogen pressure.

In order to validate the above MSR predicted results on Pt NP shapes exposed to hydrogen pressure, we searched in the literature for recent experimental results that may confirm these predicted shapes. It appears that the most commonly observed/synthesized Pt NPs structures are composed of (111) and (100) facets manifesting in cubic, octahedral, truncated octahedral and tetrahedral shapes, etc. [38–41]. Ahmadi et al. [38,39] were the first authors that reported the synthesis of Pt-NPs in the shape of cube, tetrahedron and truncated octahedron using H_2 gas flow as a reducing agent of K_2PtCl_4 in aqueous solutions wherein the shape of NPs is controlled by regulating the concentration of the capping agents. Moreover, dynamic changes of Pt NPs under hydrogen condition have been also observed in experimental works [42,43]. For example, Duan et al. [42] have reported the in-situ Cs-corrected TEM images on the supported Pt-NPs with a diameter of approximately 5 nm and have shown that Pt-NP are mainly composed of (111) and (100) planes. These authors also reported that at 473.15 K and hydrogen pressure of few mbar, the (111) surface is the main facet, while with temperature increasing to 773.15 K, a higher fraction of (100) facet was observed. All these observations are consistent with the MSR prediction results.

2.2. Mapped Environmental Segregation Energies of M-Single Atoms Embedded in Pt NPs

In order to predict the stability of M-single atoms (with M: Cu, Ag, Au, Ni, Pd, Co, Rh and Ir) embedded in the surface of Pt nanocatalysts under hydrogen reaction conditions, the environmental segregation energies E_{eseg} of M were computed in the three main facets (111), (110) and (100) of Pt NPs (Figure S2). All computed energies for the evaluation of E_{eseg} are provided in Table S2. The calculated E_{eseg} results with the predicted equilibrium NPs structures obtained by MSR model are combined, then the shape and surface composition of

M-promoted Pt NP are extrapolated under different temperatures and hydrogen pressures. The Figure 3 shows a direct picture of the main equilibrium shapes of M-promoted Pt NPs and the surface stability of the M-single atoms on different facets as a function of temperature and hydrogen pressure. The color code of the different facets represent the tendency of M-single atoms to segregate toward the surface or into the bulk: positive values of E_{eseg} superior to +0.7 eV (dark blue), between +0.7 eV and +0.3 eV (light blue) and between +0.3 eV and +0.05 eV (aqua) represent the 'very strong', 'strong' and 'weak' bulk segregation of M-single atom, respectively. This means that M cannot be found as single atom embedded on facets colored in dark blue, light blue and aqua. The negative values of E_{eseg} are inferior to −0.7 eV (red), between −0.3 eV and −0.7 eV (orange) and between −0.05 eV and −0.3 eV (yellow) represent the 'very strong', 'strong' and 'weak' surface segregation of M-single atoms, respectively. This indicates that M can be stabilized as single atom embedded on facets colored in red, orange and yellow. When E_{eseg} is between −0.05 eV and +0.05 eV (light green), promote single-atom M is considered as stable on the surface as in the bulk (no segregation preference). In the following section we describe the results obtained at 300 K, 800 K and 1200 K under 3 different hydrogen pressures (0.01, 0.1 and 1 bar) for M-single atom from coinage, nickel and cobalt groups.

2.2.1. M-Single Atoms from Coinage Group

At high temperature and low hydrogen pressure (P_{H2} = 0.01 bar and T = 1200 K), Cu as single atom is found to decorate the edges (modelled by (110) surfaces) of truncated octahedral Pt NPs. For all other considered temperature and hydrogen pressure ranges, the Cu-single atom tends to segregate towards the bulk of Pt (aqua, light- and dark-blue colors). This result is consistent with the segregation energies of Cu atoms calculated under vacuum conditions (E_{seg} = 0.42 eV in Pt (111), E_{seg} = 0.21 eV in Pt (100)) showing slight effect of the hydrogen pressure on the evolution of the chemical ordering of Pt NPs.

At high temperature (1200 K) and moderate hydrogen pressures (0.1 bar and 0.01 bar), Ag and Au single atoms are found to be stable in the surface of Pt NP (red, orange and yellow regions) with truncated octahedron shapes. This stability is lowered with increasing pressure (e.g., NP at P_{H2} = 1 bar and T = 1200 K) and decreasing temperature. With temperature continuing to decrease, Ag-single atoms are found to be stable in the Pt NP edges (yellow color are found on edges of all predicted NP shapes indicating a favorable surface segregation). From these results, one can extrapolate that for T < 800 K and under hydrogen pressure, single-Ag atoms embedded in Pt NPs can be found at the edge sites while (100) and (111) facets remain free from Ag. These results corroborate well with Jones et al. experimental observations [44] reporting that on dilute-Ag/Pt system, low-levels of Ag atoms doping in the Pt-NP surface can promote C_2H_2 to C_2H_4 hydrogenation under excess H_2 at reaction temperatures from 373 to 673 K. For Au single atom, the mapped surface segregation indicates lower stability on the surface with increasing temperature (green color) with shape evolving from near-perfect octahedral to near-perfect cube. This result is also in line with XPS analysis of Liu et al. [45], who showed that after the treatment under H_2 at 620 K of Pt surface enriched Pt-Au NP ($Pt_{80}Au_{20}$), the surface content of Au atoms is found to increase ($Pt_{61.9}Au_{38.1}$).
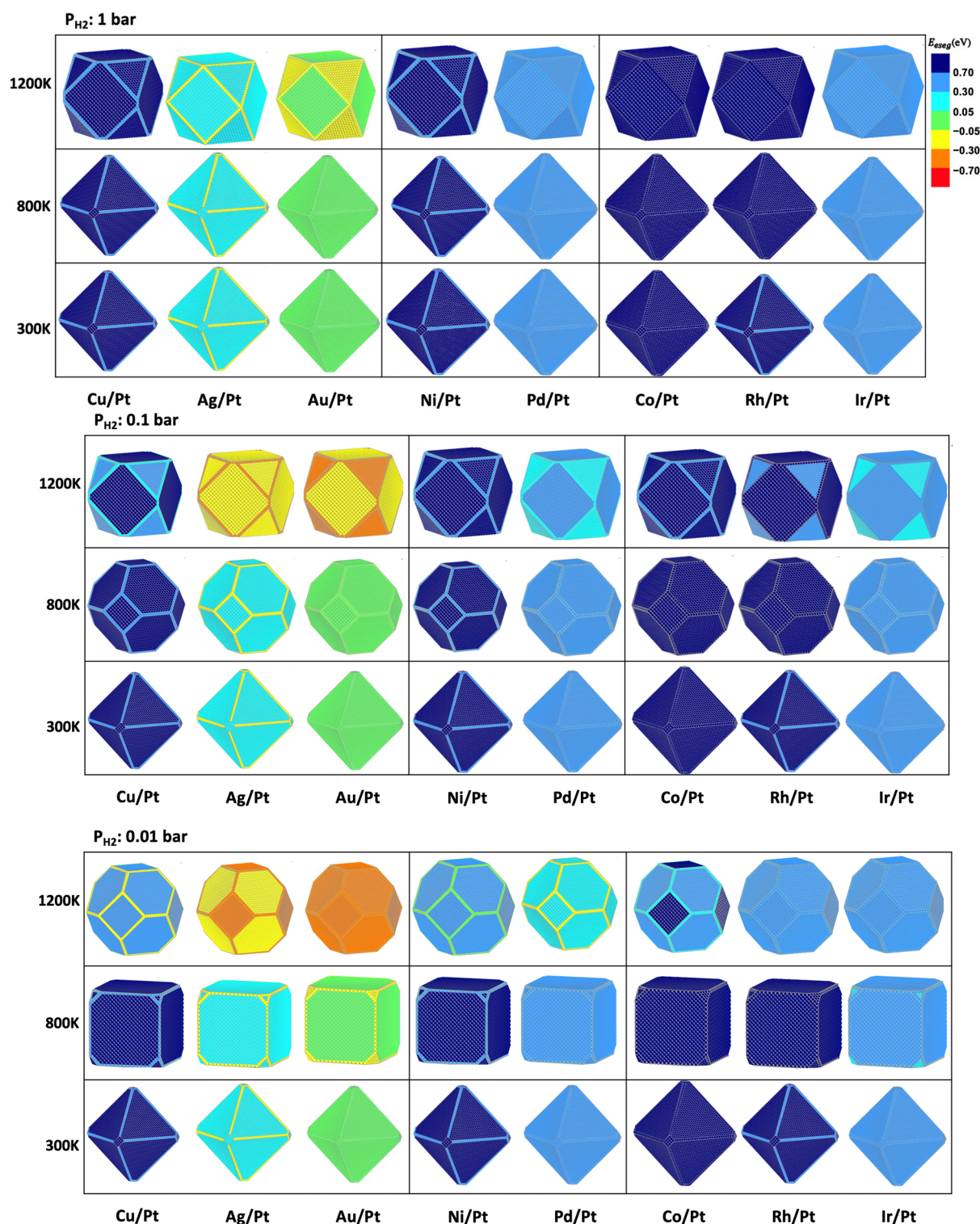
Figure 3. Color mapped environmental E$_{seg}$ and MSR predicted equilibrium M-promoted Pt NP structures along with their corresponding surface composition under 1 bar, 0.1 bar and 0.01 bar of hydrogen gas pressure.

2.2.2. M-Single Atom from Nickel Group

In contrast with the previously reported non-monotonic evolution of Pt-single atom in Ni host surfaces [31], the Ni-single atoms embedded in the Pt-NPs is found to prefer the bulk in all investigated temperature and pressure ranges. The segregation trends of

Ni-single atoms are found to be very similar to the predicted trends of Cu-single atoms. Stable in the bulk for all investigated temperature and hydrogen pressure ranges the Ni atoms may segregate towards the surface for high temperature (e.g., truncated octahedral NPs at 1200 K) and low hydrogen pressure (e.g., P_{H2} = 0.01 bar) window. The similarity of the segregation behaviors of Cu and Ni in Pt-host NPs may be linked to the smaller atomic radius (128 pm for Cu and 125 pm for Ni) compared to Pt (139 pm). Moreover, the smaller cohesive energies [46] of Cu (3.49 eV/atom) and Ni (4.44 eV/atom) compared to Pt (5.84 eV/atom), as well as the lower surface energies [22] of Ni (1.25 J/m^2) and Cu (1.28 J/m^2) over Pt (1.39 J/m^2), both favor the bulk-segregation of Cu and Ni, whereby they will have reduced strain effects and higher coordination [47].

Similar to under vacuum, single-atom Pd anchored in Pt (111) surface (E_{seg} = 0.049 eV) shows bulk-segregation preference in presence of hydrogen. The weak surface-segregation energies calculated in Pt (100) (E_{seg} = −0.12 eV) and Pt (110) (E_{seg} = −0.20 eV) surfaces under vacuum, change to negative values in presence of hydrogen indicating bulk-segregation. As it will be discussed in the next section, this counterintuitive result of the behavior of Pd in presence of hydrogen predicts a weak probability to find single Pd atoms in the surface of Pt-NPs either under vacuum or under hydrogen.

2.2.3. M-Single Atom from Cobalt Group

Under vacuum, the single-atom Co shows strong, very strong and weak bulk-segregation. The calculated segregations energies are found to be E_{seg} = 0.630 eV in Pt (111), E_{seg} = 1.010 eV in Pt (100) and E_{seg} = 0.058 eV in Pt (110) host surfaces. When exposed to hydrogen pressure and for all investigated temperature range, the Co-single atoms are found to segregate towards the bulk (dark blue, see Figure 3). This behavior is found for all Co-promoted NPs whatever the NP shapes.

Similar to Co-promoted Pt nanoparticles, in a vacuum condition, Rh and Ir single atoms are both found to be more stable in bulk-geometry than in surface when diluted into Pt (111), Pt (100) and Pt (110) facets. These predicted behaviors of the bulk segregation tendency of M-single atoms from cobalt group in Pt corroborate with several reported experimental studies [48,49] of under vacuum observations. Unfortunately, to the best of our knowledge no results are available under hydrogen pressure, making our results predictive.

2.3. Binding Hydrogen Energies

In order to understand the monitoring effect of the segregation of M-single atoms toward the surface or the bulk of Pt host NPs, we analyze the energetic parameters of the systems through the binding energy calculations on the different surface facets. Table 2 depicts the binding energies of hydrogen interacting with M-single atoms embedded in Pt (111) host surfaces. Additionally, to evaluate how M-single atoms affect their neighboring Pt atoms, the hydrogen binding energies on the neighboring Pt (with M free from hydrogen) are also reported. Interestingly, the results show that, to one exception, the calculated adsorption energies of hydrogen on Pt atom neighbors are higher than on M-single atoms embedded in Pt. In addition, except for the case of Co, the binding energies of hydrogen interacting with host Pt atoms (neighbors of anchored M-single atom) are found to be non-affected by the presence of M-single atom neighbors. Compared to Pt (111) surface (−0.7 eV), the binding energies on M-single atoms vary between +0.07 and −0.04 eV. In the histogram presentation in Figure 4 the calculated binding energies of atomic hydrogen on pure Pt (111) and M (111) surfaces are systematically included for a through comparison. Two other tables (Tables S2 and S3) and graphs (Figure S3) show calculated binding energies for the different cases (100) and (110) surfaces.

Table 2. The hydrogen binding energies on M-single atom embedded in Pt-host surfaces Pt (111) and neighboring Pt-site of M (with M free from hydrogen). Adsorption energies of hydrogen on pure Pt (111) surface were added as reference. The negative values represent exothermic adsorption energies. The endothermic adsorption energies were set to zero indicating no adsorption of hydrogen on the investigated absorption sites.

Pt (111)		Adsorption Energy −0.70 eV	
M/Pt (111)		**H Ads. on M-Single Atom/eV**	**H Ads. on Pt Neighbor/eV**
Coinage group	Cu	0.00 eV	−0.69 eV
	Ag	0.00 eV	−0.68 eV
	Au	0.00 eV	−0.66 eV
Nickel group	Ni	−0.07 eV	−0.70 eV
	Pd	−0.16 eV	−0.68 eV
Cobalt group	Co	0.00 eV	−0.17 eV
	Rh	−0.43 eV	−0.77 eV
	Ir	−0.79 eV	−0.68 eV
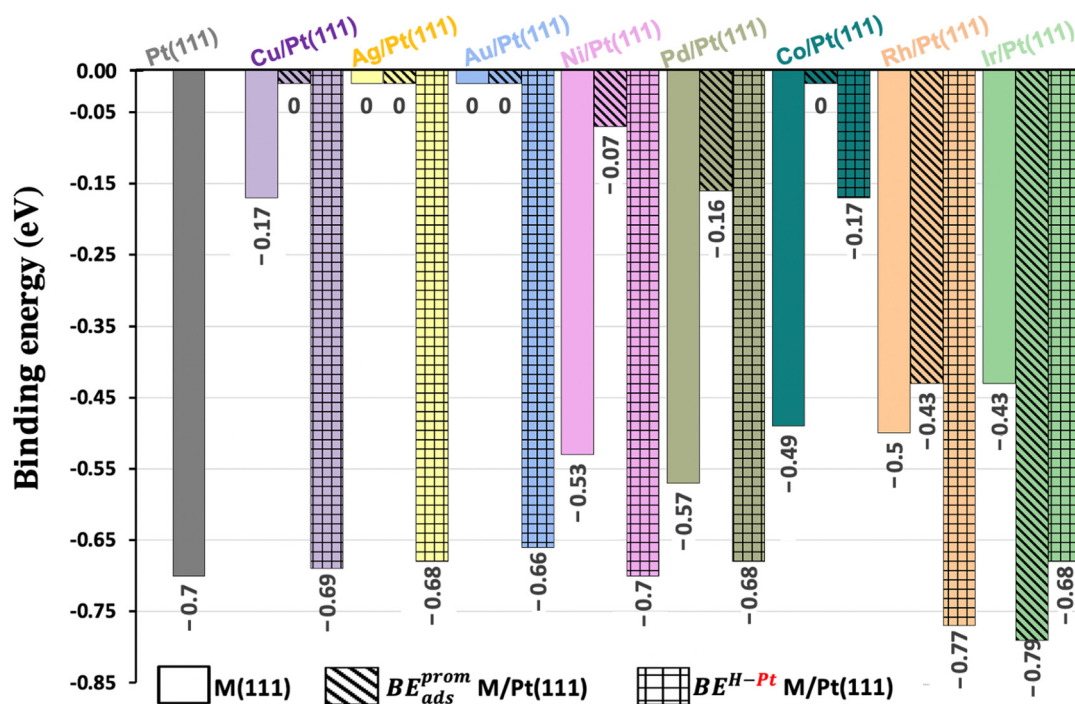
Figure 4. Hydrogen binding energy on promote M-single atom M embedded in Pt-host surfaces Pt (111) (BE$_{ads}^{SA}$, histograms filled with diagonal lines) and on the neighboring Pt-site of M (with M free of hydrogen) (BE^{H-Pt}, histograms filled in cubic-grills). The binding energy of hydrogen atom on pure Pt (111) and M (111) surfaces are added for comparison.

From this comparative histogram, one can see that among all the considered systems, only in the case of Ir-single atom embedded in the Pt (111) surface that hydrogen shows a stronger affinity to the single atom promoter than to the host Pt surface (+0.11 eV). In addition, the hydrogen is found to strongly bound to single-atom Ir with BE$_{ads}^{prom}$ = −0.79 eV while the binding energy on pure Ir (111) surface is only of −0.43 eV. In spite of this predicted strong affinity to hydrogen, no segregation toward the surface occurs in Ir-Pt (111) and the Ir single atom is found to prefer the bulk of Pt in all the studied range of hydrogen pressure. For the case of M-single atoms from the coinage group (Cu, Ag and

Au), they all show unfavorable binding energies (positive values or in case of Au/Pt (110), negligible negative value (−0.01 eV)). For Cu/Pt (111) surface, the bulk-segregation trends of single-atom Cu under vacuum is in line with its calculated endothermic hydrogen binding energy. Nevertheless, with endothermic binding to hydrogen, Au and Ag single atoms still present strong surface-segregation preference in Pt surfaces (Figure 3). These results show "counterintuitive" behavior and indicate, that the simple consideration of the affinity of one of the alloy components to the adsorbed gas phase cannot allow predicting the surface segregation or bulk segregation of M-single atoms. Similar behavior was reported, by Andersson and coworkers [50], on Cu-Pt alloy exposed to CO pressure. These authors demonstrated how CO adsorption at elevated pressures and temperatures on a Cu-Pt surface induces the segregation of the less reactive Cu component, generating a novel Cu-Pt surface alloy to which CO binds very strongly, even compared with pure Pt (111). By consequence, the segregation of single-atoms under reactive conditions will depend on many interplaying factors as the interfacial surface energies, the cohesive energies, the atomic radiuses, and the surface orientations.

3. Materials and Methods

Periodic first principles density functional theory (DFT) calculations were carried out using the Vienna Ab initio Simulation Package (VASP) [51]. Perdew, Burke, and Ernzerhof (PBE) functional [52] were used and spin polarized calculations were applied to all systems. The valence electrons were treated explicitly, and their interactions with the ionic cores were described by the projector augmented-wave method. The cut off energy was fixed to 400 eV. This value has been shown to give accurate results for the calculation of Pt system [3,10,53]. Two sizes of unit cells (3×3) and (1×1) of Pt (111), (100) and (110) surfaces were created. The surface slabs are containing 6 atomic layers from which the bottom two layers are fixed on the bulk atom positions and a vacuum space separated by 15 Å. The Brillouin zone integrations were performed with a Monkhorst–Pack ($3 \times 3 \times 1$) k-point mesh for the (3×3) unit cells and ($6 \times 6 \times 1$) k-point mesh for the (1×1) unit cells.

The morphology changes of Pt-NPs under gas environment (H_2) are quantitatively predicted by a multiscale structure reconstruction model (MSR), that has been shown to be effective for many metal nanoparticles [53–56]. This model combines DFT calculations, the Fowler-Guggenheim (F-G) adsorption isotherm [57,58] and the Wulff theorem [59]. All energetic parameters such as surface energies, interfacial energies including hydrogen adsorption energy and its evolution as a function of surface coverage are computed using DFT.

The interface tension γ_{hkl}^{int} (Equation (1)) is calculated as the sum of the term of surface energy γ_{hkl} calculated under vacuum and the term of the coverage of gas adsorbates.

$$\gamma_{hkl}^{int} = \gamma_{hkl} + \theta \left(\frac{E_{ads}^{hkl}}{A} \right) \tag{1}$$

where A is the surface area per atom, and E_{ads}^{hkl} is the gas adsorption energy on the surface. The average coordination number ($\overline{CN}$) descriptor is selected to identify the different shapes of constructed NPs. These values are obtained by calculating the total CN of all the atoms located on the NP surface divided by the number of sites:

$$\overline{CN} = \frac{\sum_{i=1}^{N_{surf}} CN_i}{N_{surf}} \tag{2}$$

where CN_i is the surface coordination number of ith atom, and N_{surf} is the number of atoms located on the surface of constructed nanoparticles. Each $\overline{CN}$ value that satisfies $\overline{CN} > 0.1$ represents a new NP shape. For more details, see ref. [54–56].

To map the surface segregation evolution of M-single atoms (SA) embedded in the Pt surfaces as a function of the temperature and hydrogen pressure, the environmental segregation energy (E_{eseg}) was calculated as following:

$$E_{eseg} = E_{seg} + \left(E_{ads}^{SA} \theta_{SA} - E_{ads}^{host} \theta_{host} \right) \tag{3}$$

with,

$$E_{seg} = E_{surf}^{SA} - E_{bulk}^{SA} \tag{4}$$

where E_{seg} is the energy difference between an initial system where the M-single atom (M = transition metals) is anchored in the bulk (E_{bulk}^{SA}) of the host (Pt) slab and a final system where M-single atom is anchored in the top layer (E_{surf}^{SA}) of the host (Pt) slab. The embedding of M-single atom in Pt host surface (9 atoms by layer) corresponds to a surface concentration of 11%. If E_{seg} is sufficiently negative, the M-single atom segregates to the surface, and when E_{seg} is sufficiently positive it segregates to the bulk. E_{ads}^{SA}, E_{ads}^{host} are average hydrogen adsorption energies on the M-single atom and on the surface host (Pt) site, respectively, while θ_{SA} and θ_{host} are the gas adsorption coverage (θ) on surface M single atom and on surface Pt-host site, respectively. The adsorption energy for E_{eseg} model is corrected as:

$$E_{ads}^{host} = BE^{host} - zw\theta_{host} \tag{5}$$

$$E_{ads}^{SA} = BE^{SA} - zw\theta_{host} \tag{6}$$

where the BE^{host} is selected as the most stable adsorption energy of one hydrogen (H) atom on the clean host (Pt) surface. BE^{SA} is adsorption energy of one H atom on the top site of isolated M-single atom embedded in the host (Pt) surface. zw lateral interactions were evaluated as the hydrogen adsorption energy difference between the (1×1) and (3×3) M-host surfaces, representing full adsorbates coverage ($\theta_H = 1$) and extremely low coverage ($\theta_H = 1/9$), respectively.

Following the Fowler-Guggenheim (F-G) adsorption formalism the evolution of hydrogen coverage on single-atom M site (θ_H^{single}) and on host atom Pt (θ_H^{host}) may be expressed as follows:

$$PK = \frac{\theta_H^{host/single}}{1 - \theta_H^{host/single}} e^{-c\theta_H^{host}}, c = \frac{zw}{RT} \tag{7}$$

$$K = \exp\left(-\frac{BE^{host/single} - T\left(S_{ads} - S_{gas}\right)}{RT} \right) \tag{8}$$

where K is the adsorption equilibrium constant, S_{ads} is the entropy of adsorbed gas assumed to stick on the surface and thus considered to be equal to zero, and S_{gas} is the entropy of hydrogen gas phase molecule for which the values are fitted based on the data from the NIST-JANAF Thermochemical Tables [60]. More methodological details could be found in previous works [25,61].

Using these two models combined with DFT computed energetics, the shape and segregation trends of 8 different M-promoted Pt nanostructured catalysts evolving under varied temperatures and hydrogen pressures are predicted.

4. Conclusions

The shape and surface composition of bimetallic nanoalloys are dynamically changing under varied temperature and gas pressure. In this work, by combining DFT calculations, Wulff constructions and Fowler-Guggenheim theorem, the environmental segregation model, the shape and the stability of 8 different M-promoted Pt NPs under different temperatures and hydrogen pressures were calculated and predicted. The results revealed two different evolution manners of the shape of M-promoted Pt systems: (i) for $P_{H2} > 10^4$ Pa, the NP shape evolves gradually with increasing temperature from near-perfect octahe-

dron to near-perfect cube shape with reducing the proportion of the (111) surface while increasing the proportion of the (100). Furthermore, (ii) for $P_{H2} < 10^4$ Pa, the Pt-NP is found to undergo reversible shape changes and many possible shapes could be stabilized as a function of temperature.

Considering the stability of M-single atoms embedded in Pt NPs studied through the environmental segregation model, the results show that only Ag and Au single atom promoters are found to segregate toward the surface of Pt under hydrogen. All other promoters are found to be stable in the bulk of Pt NPs. These results show how the segregation behavior in presence of reactive gas is a complex process happening in bimetallic alloys. The simplistic picture, in which the response to adsorbates is that the more reactive alloy component (i.e., the one interacting strongly with the adsorbates) segregates to the surface, may induce erroneous interpretations. The reality is that the chemistry of diluted single atoms in Pt is completely different from what is known from the extended surfaces and from clusters and nanoparticle. The stability of M-single atoms is an interplay between different alloy properties and depends either on their modified electronic structure within the host material, their geometric ensemble (surface orientation) and on their affinity to the reactive gas. In addition, adsorption and diffusion of hydrogen in the inner layers of Pt NPs may play a role in the stability of the M promoters and the shape of the catalysts. These considerations need further experimental and theoretical investigations.

References

1. Yu, W.; Porosoff, M.D.; Chen, J.G. Review of Pt-based bimetallic catalysis: From model surfaces to supported catalysts. *Chem. Rev.* **2012**, *112*, 5780–5817. [CrossRef] [PubMed]
2. Bandarenka, A.S.; Koper, M.T.M. Structural and electronic effects in heterogeneous electrocatalysis: Toward a rational design of electrocatalysts. *J. Catal.* **2013**, *308*, 11–24. [CrossRef]
3. Dimitrova, N.; Dhifallah, M.; Mineva, T.; Boiadjieva-Scherzer, T.; Guesmi, H.; Georgieva, J. High performance of PtCu@TiO2 nanocatalysts toward methanol oxidation reaction: From synthesis to molecular picture insight. *RSC Adv.* **2019**, *9*, 2073–2080. [CrossRef] [PubMed]
4. Liu, Y.; Zha, M.; Qin, H.; Yao, S.; Zhou, X.; Zhao, S.; Sheng, N.; Sun, Y.; Jin, X.; Yan, H.; et al. Au-Promoted Pt nanoparticles supported on MgO/SBA-15 as an efficient catalyst for selective oxidation of glycerol. *AlChE J.* **2021**, *67*, e17196. [CrossRef]
5. Yang, K.; Yang, B. Surface restructuring of Cu-based single-atom alloy catalysts under reaction conditions: The essential role of adsorbates. *Phys. Chem. Chem. Phys.* **2017**, *19*, 18010–18017. [CrossRef]
6. Yang, K.; Yang, B. Identification of the Active and Selective Sites over a Single Pt Atom-Alloyed Cu Catalyst for the Hydrogenation of 1,3-Butadiene: A Combined DFT and Microkinetic Modeling Study. *J. Phys. Chem. C* **2018**, *122*, 10883–10891. [CrossRef]
7. Wang, Q.; Nassereddine, A.; Loffreda, D.; Ricolleau, C.; Alloyeau, D.; Louis, C.; Delannoy, L.; Nelayah, J.; Guesmi, H. Cu segregation in Au-Cu nanoparticles exposed to hydrogen atmospheric pressure: How is fcc symmetry maintained? *Faraday Discuss.* **2022**, *advance article*. [CrossRef]
8. Nassereddine, A.; Wang, Q.; Loffreda, D.; Ricolleau, C.; Alloyeau, D.; Louis, C.; Delannoy, L.; Nelayah, J.; Guesmi, H. Revealing size-dependent structural transition in supported gold nanoparticles at atmospheric pressure. *Small* **2021**, *17*, 2104571. [CrossRef]
9. Khelfa, A.; Meng, J.; Byun, C.; Wang, G.; Ricolleau, C.; Nelayah, J.; Amara, H.; Guesmi, H.; Alloyeau, D. Selective shortening of gold nanorods: When surface functionalization dictates the reactivity of nanostructures. *Nanoscale* **2020**, *12–44*, 22658–22667. [CrossRef]
10. Wisniewska, J.; Guesmi, H.; Ziolek, M.; Tielens, T. Stability of nanostructured Silver-Platinum alloys. *J. Alloys Comp.* **2019**, *760*, 934–941. [CrossRef]
11. Chakrabarti, A.; Ford, M.E.; Gregory, D.; Hu, R.; Keturakis, C.J.; Lwin, S.; Tang, Y.; Yang, Z.; Zhu, M.; Bañares, M.A.; et al. A decade+ of operando spectroscopy studies. *Catal. Today* **2017**, *283*, 27–53. [CrossRef]
12. Weckhuysen, B.M. Studying birth, life and death of catalytic solids with operando spectroscopy. *Natl. Sci. Rev.* **2015**, *2*, 147–149. [CrossRef]
13. Jones, C.W.; Tao, F.; Garland, M.V. Introduction to Special Issue on Operando and In Situ Studies of Catalysis. *ACS Catal.* **2012**, *2*, 2444–2445. [CrossRef]
14. Ahmadi, M.; Cui, C.; Mistry, H.; Strasser, P.; Cuenya, B.R. Carbon Monoxide-Induced Stability and Atomic Segregation Phenomena in Shape-Selected Octahedral PtNi Nanoparticles. *ACS Nano* **2015**, *9*, 10686–10694. [CrossRef]
15. Tao, F.; Grass, M.E.; Zhang, Y.; Butcher, D.R.; Renzas, J.R.; Liu, Z.; Chung, J.Y.; Mun, B.S.; Salmeron, M.; Somorjai, G.A. Reaction-driven restructuring of Rh-Pd and Pt-Pd core-shell nanoparticles. *Science* **2008**, *322*, 932–934. [CrossRef]
16. Mu, R.T.; Guo, X.G.; Fu, Q.; Bao, X.H. Oscillation of Surface Structure and Reactivity of PtNi Bimetallic Catalysts with Redox Treatments at Variable Temperatures. *J. Phys. Chem. C* **2011**, *115*, 20590–20595. [CrossRef]
17. Bergmann, A.; Roldan Cuenya, B. Operando Insights into Nanoparticle Transformations during Catalysis. *ACS Catal.* **2019**, *9*, 10020–10043. [CrossRef]
18. Wang, Q.; Tichit, D.; Meunier, F.; Guesmi, H. Combined DRIFTS and DFT Study of CO Adsorption and Segregation Modes in Pt-Sn Nanoalloys. *J. Phys. Chem. C* **2020**, *124*, 9979–9989. [CrossRef]
19. Guesmi, H.; Louis, C.; Delannoy, L. Chemisorbed atomic oxygen inducing Pd segregation in PdAu (111) alloy: Energetic and electronic DFT analysis. *Chem. Phys. Lett.* **2011**, *503*, 97–100. [CrossRef]
20. Dhouib, A.; Guesmi, H. DFT study of the M segregation on MAu alloys (M=Ni, Pd, Pt) in presence of adsorbed oxygen O and O2. *Chem. Phys. Lett.* **2012**, *521*, 98–103. [CrossRef]
21. Guesmi, H. Theoretical insights on the effect of reactive gas on the chemical ordering of gold-based alloys. *Gold Bull.* **2013**, *46*, 213–219. [CrossRef]
22. Sansa, M.; Dhouib, A.; Guesmi, H. Density functional theory study of CO-induced segregation in gold-based alloys. *J. Chem. Phys.* **2014**, *141*, 064709. [CrossRef] [PubMed]
23. Ruban, A.V.; Skriver, H.L.; Norskov, J.K. Surface segregation energies in transition-metal alloys. *Phys. Rev. B* **1999**, *59*, 15990–16000. [CrossRef]
24. Greeley, J.; Mavrikakis, M. Alloy catalysts designed from first principles. *Nat. Mater.* **2004**, *3*, 810–815. [CrossRef] [PubMed]
25. Meng, J.; Zhu, B.E.; Gao, Y. Surface Composition Evolution of Bimetallic Alloys under Reaction Conditions. *J. Phys. Chem. C* **2019**, *123*, 28241–28247. [CrossRef]
26. Mostafa, S.; Behafarid, F.; Croy, J.R.; Ono, L.K.; Li, L.; Yang, J.C.; Frenkel, A.I.; Cuenya, B.R. Shape-dependent catalytic properties of Pt nanoparticles. *J. Am. Chem. Soc.* **2010**, *132*, 15714–15719. [CrossRef]
27. Mavrikakis, M.; Stoltze, P.; Nørskov, J.K. Making Gold Less Noble. *Catal. Lett.* **2000**, *64*, 101–106. [CrossRef]
28. Lopez, N.; Janssens, T.V.W.; Clausen, B.S.; Xu, Y.; Mavrikakis, M.; Bligaard, T.; Norskov, J.K. On the origin of the catalytic activity of gold nanoparticles for low-temperature CO oxidation. *J. Catal.* **2004**, *223*, 232–235. [CrossRef]

29. Norskov, J.K.; Bligaard, T.; Hvolbaek, B.; Abild-Pedersen, F.; Chorkendorff, I.; Christensen, C.H. The nature of the active site in heterogeneous metal catalysis. *Chem. Soc. Rev.* **2008**, *37*, 2163–2171. [CrossRef]

30. Komanicky, V.; Iddir, H.; Chang, K.C.; Menzel, A.; Karapetrov, G.; Hennessy, D.; Zapol, P.; You, H. Shape-dependent activity of platinum array catalyst. *J. Am. Chem. Soc.* **2009**, *131*, 5732–5733. [CrossRef]

31. Mistry, H.; Behafarid, F.; Zhou, E.; Ono, L.K.; Zhang, L.; Roldan Cuenya, B. Shape-Dependent Catalytic Oxidation of 2-Butanol over Pt Nanoparticles Supported on γ-Al2O3. *ACS Catal.* **2014**, *4*, 109–115. [CrossRef]

32. Vitos, L.; Ruban, A.V.; Skriver, H.L.; Kollar, J. The surface energy of metals. *Surf. Sci.* **1998**, *411*, 186–202. [CrossRef]

33. Tran, R.; Xu, Z.; Radhakrishnan, B.; Winston, D.; Sun, W.; Persson, K.A.; Ong, S.P. Surface energies of elemental crystals. *Sci. Data* **2016**, *3*, 160080. [CrossRef] [PubMed]

34. Yu, Y.; Yang, J.; Hao, C.; Zhao, X.; Wang, Z. The Adsorption, Vibration and Diffusion of Hydrogen Atoms on Platinum Low-Index Surfaces. *J. Comput. Theor. Nanosci.* **2009**, *6*, 439–448. [CrossRef]

35. Shi, Q.; Sun, R. Adsorption manners of hydrogen on Pt (100), (110) and (111) surfaces at high coverage. *Comput. Theor. Chem.* **2017**, *1106*, 43–49. [CrossRef]

36. Bernard Rodriguez, C.R.; Santana, J.A. Adsorption and diffusion of sulfur on the (111), (100), (110), and (211) surfaces of FCC metals: Density functional theory calculations. *J. Chem. Phys.* **2018**, *149*, 204701. [CrossRef] [PubMed]

37. Garcia-Araez, N. Enthalpic and Entropic Effects on Hydrogen and OH Adsorption on Pt (111), Pt (100), and Pt (110) Electrodes As Evaluated by Gibbs Thermodynamics. *J. Phys. Chem. C* **2010**, *115*, 501–510. [CrossRef]

38. Ahmadi, T.S.; Wang, Z.L.; Green, T.C.; Henglein, A.; El-Sayed, M.A. Shape-Controlled Synthesis of Colloidal Platinum Nanoparticles. *Science* **1996**, *272*, 1924–1926. [CrossRef]

39. Ahmadi, T.S.; Wang, Z.L.; Henglein, A.; El-Sayed, M.A. "Cubic" Colloidal Platinum Nanoparticles. *Chem. Mater.* **1996**, *8*, 1161–1163. [CrossRef]

40. Song, H.; Kim, F.; Connor, S.; Somorjai, G.A.; Yang, P. Pt nanocrystals: Shape control and Langmuir-Blodgett monolayer formation. *J. Phys. Chem. B* **2005**, *109*, 188–193. [CrossRef]

41. Bratlie, K.M.; Lee, H.; Komvopoulos, K.; Yang, P.; Somorjai, G.A. Platinum nanoparticle shape effects on benzene hydrogenation selectivity. *Nano Lett.* **2007**, *7*, 3097–3101. [CrossRef]

42. Duan, M.; Yu, J.; Meng, J.; Zhu, B.; Wang, Y.; Gao, Y. Reconstruction of Supported Metal Nanoparticles in Reaction Conditions. *Angew. Chem. Int. Ed. Engl.* **2018**, *57*, 6464–6469. [CrossRef] [PubMed]

43. Shi, Y.; Lyu, Z.; Zhao, M.; Chen, R.; Nguyen, Q.N.; Xia, Y. Noble-Metal Nanocrystals with Controlled Shapes for Catalytic and Electrocatalytic Applications. *Chem. Rev.* **2021**, *121*, 649–735. [CrossRef] [PubMed]

44. Jones, L.C.; Buras, Z.; Gordon, M.J. Partial Hydrogenation of C2H2 on Ag-Doped Pt Nanoparticles. *J. Phys. Chem. C* **2012**, *116*, 12982–12988. [CrossRef]

45. Liu, C.W.; Wei, Y.C.; Wang, K.W. Promotion of ceria-modified Pt-Au/C cathode catalysts for oxygen reduction reaction by H2-induced surface segregation. *Chem. Commun.* **2010**, *46*, 2483–2485. [CrossRef]

46. Kittel, C.; McEuen, P. *Introduction to Solid State Physics*; John Wiley & Sons: Hoboken, NJ, USA, 2015.

47. Gould, A.L.; Heard, C.J.; Logsdail, A.J.; Catlow, C.R. Segregation effects on the properties of (AuAg)147. *Phys. Chem. Chem. Phys.* **2014**, *16*, 21049–21061. [CrossRef]

48. Williams, F.L.; Nelson, G.C. Surface composition of Pt/Rh alloys. *Appl. Surf. Sci.* **1979**, *3*, 409–415. [CrossRef]

49. Van Delft, F.C.M.J.M.; Van Langeveld, A.D.; Nieuwenhuys, B.E. The temperature dependence of the surface composition of Pt−Rh alloys. *Surf. Sci.* **1987**, *189–190*, 1129–1134. [CrossRef]

50. Andersson, K.J.; Calle-Vallejo, F.; Rossmeisl, J.; Chorkendorff, I. Adsorption-Driven Surface Segregation of the Less Reactive Alloy Component. *J. Am. Chem. Soc.* **2009**, *131*, 2404–2407. [CrossRef]

51. Kresse, G.; Hafner, J. Ab initio molecular dynamics for liquid metals. *Phys. Rev. B* **1993**, *47*, 558–561. [CrossRef]

52. Perdew, J.P.; Wang, Y. Accurate and simple analytic representation of the electron-gas correlation energy. *Phys. Rev. B* **1992**, *45*, 13244–13249. [CrossRef]

53. Raybaud, P.; Chizallet, C.; Mager-Maury, C.; Digne, M. Toulhoat, M.; Sautet, P. From γ-alumina to supported platinum nanoclusters in reforming conditions: 10 years of DFT modeling and beyond. *J. Catal.* **2013**, *308*, 328–340. [CrossRef]

54. Chmielewski, A.; Meng, J.; Zhu, B.; Gao, Y.; Guesmi, H.; Prunier, H.; Alloyeau, D.; Wang, G.; Louis, C.; Delannoy, L.; et al. Reshaping Dynamics of Gold Nanoparticles under H2 and O2 at Atmospheric Pressure. *ACS Nano* **2019**, *13*, 2024–2033. [CrossRef] [PubMed]

55. Zhu, B.; Meng, J.; Gao, Y. Equilibrium Shape of Metal Nanoparticles under Reactive Gas Conditions. *J. Phys. Chem. C* **2017**, *121*, 5629–5634. [CrossRef]

56. Zhu, B.; Xu, Z.; Wang, C.; Gao, Y. Shape Evolution of Metal Nanoparticles in Water Vapor Environment. *Nano Lett.* **2016**, *16*, 2628–2632. [CrossRef]

57. Langmuir, I. The Adsorption of Gases on Plane Surfaces of Glass, Mica and Platinum. *J. Am. Chem. Soc.* **1918**, *40*, 1361–1403. [CrossRef]

58. Fowler, R.H.; Guggenheim, E.A. *Statistical Thermodynamics*; Cambridge University Press: Cambridge, UK, 1939.

59. Wulff, G. Zur Frage der Geschwindigkeit des Wachsthums und der Auflösung der Krystallflächen. *Z. Kristallogr. Cryst. Mater.* **1901**, *34*, 449. [CrossRef]

60. Chase, M.W.; Davies, C.A.; Downey, J.R.; Frurip, D.J., Jr.; McDonald, R.A.; Syverud, A.N. Nist-Janaf Thermochemical Tables. Available online: https://janaf.nist.gov/ (accessed on 13 March 2022).

61. Wang, Q.; Zhu, B.; Tielens, F.; Tichit, D.; Guesmi, H. Mapping Surface Segregation of Single-Atom Pt Dispersed in M Surfaces (M = Cu, Ag, Au, Ni, Pd, Co, Rh and Ir) Under Hydrogen Pressure at Various Temperatures. *Appl. Surf. Sci.* **2021**, *548*, 149217. [CrossRef]